Roof Retrofit Scenarios for Thermally Vulnerable Homes: A CFD-Based Study of Indoor Thermal Performance in San Antonio, Texas

Quang Van Tran*, *Farzad* Hashemi*, *Parisa* Najafian, and *Esteban López* Ochoa

School of Architecture and Planning, The University of Texas at San Antonio, TX 78205, USA

Abstract. In the hot and humid climate of San Antonio, Texas, residential buildings consume approximately 43 percent of the city's electricity. Yet older, heat-vulnerable homes, particularly in lower-income neighborhoods, remain largely underserved in energy efficiency efforts, as local government weatherization programs mainly provide standardized solutions that require the building envelope to be in good condition. Roofs are the most exposed elements in the envelope and strongly influence heat gain and indoor conditions. This study assesses the thermal performance of roof retrofit scenarios in an older, detached single-family home representative of this underserved housing stock. We employed a transient Computational Fluid Dynamics (CFD) model developed in ANSYS Fluent to simulate unsteady indoor airflow using the Stress-Blended Eddy Simulation (SBES) turbulence model and the P1 radiation approach for radiative heat exchange. Four roof-albedo scenarios (α = 0.20, 0.40, 0.60, 0.80) were evaluated under typical summer conditions representative of passive ventilation periods. Model validation against on-site sensor data achieved coefficients of determination of 0.90 for air temperature and 0.89 for velocity, confirming strong predictive accuracy. Increasing roof albedo from 0.20 to 0.80 reduced roof heat absorption by approximately 75%, decreased conductive heat transfer by 60%, and lowered indoor peak temperature by 0.8°C, shortening exposure above 32°C by roughly 20%. Complementary drone thermal imagery collected using DJI Matrice 350 RTK corroborated substantial surface-temperature reductions between dark and reflective roofs transitions funded by the City of San Antonio's Cool Roof Program. The findings demonstrate that high-albedo cool roofs represent a cost-effective and scalable retrofit strategy to mitigate indoor overheating and energy burden in ASHRAE Climate Zone 2A, advancing equitable climate adaptation and housing resilience.

Keywords. Cool roofs, Thermal comfort, CFD, Heat-vulnerable homes

1 Introduction

Addressing climate change and rising urban temperatures requires improving the energy performance of buildings through targeted and sustainable design interventions. Among the various building envelope components, roofs play a particularly influential role because they receive the highest exposure to solar radiation. This exposure results in significant heat gain within buildings and contributes to the urban heat island effect, particularly in low-insulated dwellings. Passive retrofit solutions, such as cool roofs and green roofs, have therefore gained prominence for their capacity to reduce heat accumulation and enhance thermal performance [1]. Cool roofs, in particular, increase surface reflectivity and minimize solar heat absorption, thereby lowering cooling energy demand and indoor heat stress [2,3]. Despite documented benefits, roof retrofitting remains underutilized in most urban contexts [4], representing a significant opportunity to enhance energy efficiency and thermal resilience, particularly in dense built environments [5].

Cool roofs reduce building energy consumption primarily through increased surface albedo. By reflecting a greater proportion of incoming solar radiation, these coatings lower roof surface temperatures and reduce conductive heat transfer into buildings. Empirical and modeling studies demonstrate that this mechanism yields appreciable year-round benefits in hot, sun-dominated climates. For instance, increasing roof albedo from 0.2 to 0.8 in Dubai produced substantial reductions in both cooling and heating loads, an average energy decline of 32.16% for uninsulated buildings and 24.3% for insulated buildings, highlighting pronounced potential for net annual savings in subtropical desert contexts [6]. Similarly, Seifhashemi et al. (2018) [7] report consistent cooling-season savings for single-story retail warehouses across Australian climate zones, with annual reductions of 6.5–8.4 kWh.m^{-2}. The most significant effects occurred in tropical, subtropical, and arid regions. These findings align with broader evidence indicating that reflective roof treatments can substantially lower surface and near-roof air temperatures, thereby reducing peak cooling demand during periods of high solar irradiance [8,9].

However, the effectiveness of cool roofs varies across contexts. Local climate, building envelope insulation, urban geometry, and interactions with other mitigation measures all influence outcomes. Elnabawi et al. (2023) [8] demonstrate that very high-albedo "super cool" coatings can outperform conventional cool and vegetated roofs in reducing mean radiant temperature and physiologically equivalent temperature at the

* Corresponding author: quangvan.tran@utsa.edu; farzad.hashemi@utsa.edu

© The Authors, published by EDP Sciences. This is an open access article distributed under the terms of the Creative Commons Attribution License 4.0 (https://creativecommons.org/licenses/by/4.0/).

neighborhood scale, particularly in hot-arid settings. Conversely, Yang et al. (2025) [9] emphasize that multi-criteria assessments, combining energy performance, microclimate impacts, life-cycle costs, and technical feasibility, prove essential for robust retrofit decisions in temperate urban contexts. These studies suggest that while cool roofs offer clear thermodynamic advantages in many warm climates, decision-makers should evaluate albedo upgrades alongside green-roof alternatives and site-specific constraints to identify the most effective and equitable retrofit strategy. Despite extensive research on cool roofs at urban and building scales, few studies have examined their effectiveness in thermally vulnerable and under-insulated residential buildings using high-fidelity transient CFD analysis. This gap is critical because low-income and aging housing stock, common in hot-humid regions, experiences disproportionate heat stress and energy burden, yet remains underserved in retrofit programs. To address this gap, this study applies transient computational fluid dynamics (CFD) using the stress-blended eddy simulation (SBES) model coupled with P-1 radiation modeling to capture buoyancy-driven, low-velocity indoor thermal dynamics at high spatial resolution. The objectives are to: (1) evaluate the indoor thermal performance of four roof-albedo scenarios (α= 0.20, 0.40, 0.60, 0.80) under typical passive-ventilation conditions; (2) quantify spatial and temporal variations in indoor air temperature within a representative 1970s-era dwelling in San Antonio, Texas; and (3) assess the potential of high-albedo roof retrofits for reducing thermal stress and energy burden in heat-vulnerable households. This study contributes to ongoing research on equitable and evidence-based passive cooling strategies, providing quantitative guidance for cost-effective retrofits in hot-humid climates.

2 Methodology

2.1. Study area and case study selection

San Antonio, the second-largest city in Texas, contains a substantial inventory of under-insulated, air-conditioning-dependent homes constructed during the 1970s and 1980s energy crisis. These residences concentrate in historically underserved neighborhoods, particularly on the Westside (Figure 1). The aging wood-framed housing stock exhibits significant physical deterioration after several decades of operation, resulting in substantial energy burdens for residents [10]. This study examines a representative single-family dwelling that is typical of this housing typology to evaluate roof retrofit strategies for improving indoor thermal performance.

The case study dwelling represents a single-story wood-frame structure with a floor area of 70 m² and a height of 4.6 m. The building envelope exhibits minimal window-to-wall ratios across all orientations: north (2.40%), south (8.76%), west (4.20%), and east (1.66%). Figure 1 presents the multi-scale representation of the dwelling, from its regional context to the computational model geometry.

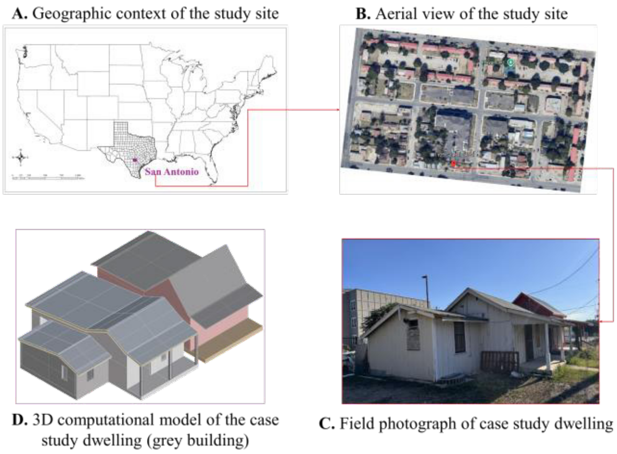

Fig.1. Multi-Scale Representation of the Case Study Dwelling: From Regional Context to Computational Model

This study evaluates four roof retrofit strategies differentiated by surface albedo values ranging from 0.2 to 0.8. Scenario 1 (albedo = 0.2) represents the baseline condition, where conventional dark asphalt shingles exhibit high solar absorptivity (0.8), resulting in a substantial heat flux through the roof assembly into the conditioned space. Scenarios 2 and 3 (albedo = 0.4 and 0.6, respectively) represent intermediate retrofit options achievable through medium-reflectance coatings or lighter-colored roofing materials, progressively reducing solar heat gain. Scenario 4 (albedo = 0.8) represents a high-performance cool roof coating that reflects 80% of incident solar radiation, absorbing only 20% and thereby minimizing conductive heat transfer through the building envelope. All scenarios maintained identical roof assemblies, isolating albedo as the sole variable, and were simulated over a 24-h diurnal cycle under representative summer conditions (Fig. 2).

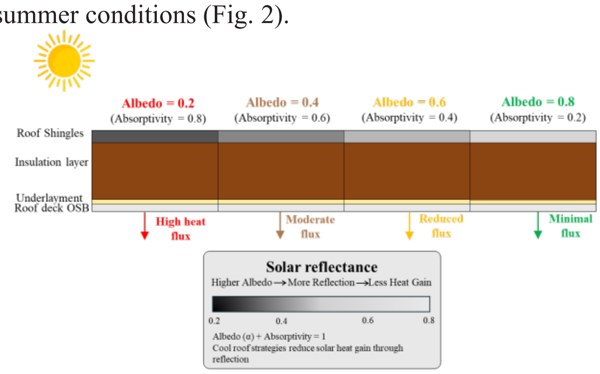

Fig.2. Roof retrofit scenarios based on surface albedo modification

2.2. Computational domain and boundary conditions

2.2.1. Domain configuration

The computational domain follows established guidelines for building aerodynamics simulations [4,5]. The computational domain extends 5H upstream of the dwelling, 15H downstream, and ±5H laterally, with the domain top located 5H above ground level (Fig. 3). Here, H denotes the characteristic maximum building height of the case dwelling, measured from ground to the roof ridge (H = 4.6 m); the heights range from 2.9–4.6 m. Figure 3 illustrates the domain configuration and dimensions.

Symmetry boundary conditions apply to the lateral boundaries and the top of the domain. The inlet implements atmospheric boundary layer profiles for velocity, turbulent kinetic energy, and turbulent dissipation rate. The outlet maintains a fixed static pressure condition. Ground and building surfaces employ no-slip wall conditions with standard wall functions.

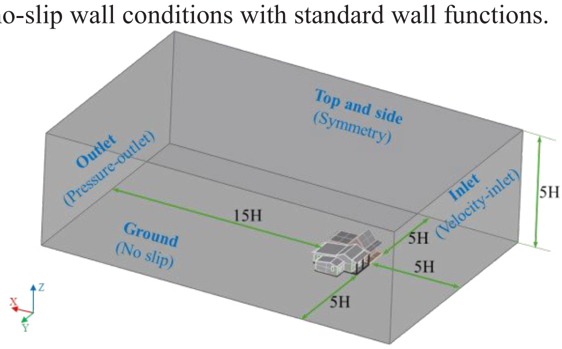

Fig.3. Schematic diagram of the computational domain (H=4.6, height of the building)

2.2.2. Atmospheric boundary layer profile

The inlet velocity profile follows the logarithmic law [11]

$$U(z)=\frac{u_*}{k}\times\ln\left(\frac{z+z_0}{z_0}\right) \quad (1)$$

where z represents the height above ground, z_0 denotes the aerodynamic roughness length (0.03 m for the ground to fit with the experimental on-site weather station), k is the von Karman constant (0.42), and u_* represents the friction velocity.

2.2.3. Continuous phase simulation

Airflow and heat transfer in the domain were simulated transiently using the stress-blended eddy simulation (SBES) turbulence model based on the SST k–ω formulation.

Continuity Equation

$$\frac{\partial\rho}{\partial t}+\frac{\partial(\rho u_i)}{\partial x_i}=0 \quad (2)$$

Momentum Equation

$$\frac{\partial(\rho u_i)}{\partial t}+\frac{\partial(\rho u_i u_j)}{\partial x_j}=-\frac{\partial p}{\partial x_j}+\frac{\partial}{\partial x_j}\left[\mu_0\left(\frac{\partial u_i}{\partial x_j}+\frac{\partial u_j}{\partial x_i}\right)\right]-\beta g\rho\Delta T\delta_{ij}$$

(3)

Energy Equation

$$\frac{\partial(\rho T)}{\partial t}+\frac{\partial(\rho u_i T)}{\partial x_i}=\frac{\partial}{\partial x_i}\left(\Gamma_T\frac{\partial T}{\partial x_i}\right)+\frac{Q_T}{c_P}+\frac{1}{c_P}\left(\frac{\partial q_{ri}}{\partial x_i}\right) \quad (4)$$

Where u_i and u_j are the velocity components in the direction i and j of Cartesian coordinates. δ_{ij} is the Kronecker delta. ρ is fluid density and p is pressure.

$\mu_0=\mu+\mu_t$, $\beta=1/T_{ref}$, $\Gamma_T=\frac{\mu}{P_r}+\frac{\mu_t}{P_{rt}}$

SBES Turbulent Viscosity

$$\mu_t^{SBES}=f_{SBES}\cdot\mu_t^{RANS}+(1-f_{SBES})\cdot\mu_t^{LES} \quad (5)$$

Where $\mu_t^{RANS}=\frac{\rho a_1 k}{\max(a_1\omega,SF_2)}$ and $\mu_t^{LES}=\rho(C_{SBES}\Delta)^2 S$

P-1 Radiative Transfer Equation

$$\nabla\cdot(\Gamma\nabla G)-aG+4a\sigma T^4=S_G \quad (6)$$

Where $\Gamma=\frac{1}{3(a+\sigma_s)}$ and $q_r=-\Gamma\nabla G$

Wall heat balance

$$q_{cond}=q_{conv}+q_{rad,solar}+q_{rad,thermal}$$

(7)

Where $q_{rad,solar}=\alpha\cdot I_{solar}$

$q_{conv}=h_c(T_{wall}-T_{air})$

$qrad,thermal=\varepsilon\sigma T_{wall}^4-\varepsilon G$

Albedo-Absorptivity Relationship

$$\alpha+\rho_{ref}=1 \quad (8)$$

2.3. Mesh design and grid independence analysis

The computational domain utilizes hexahedral elements in the Fluent Meshing model (ANSYS Inc.) with 10 prism layers adjacent to the building walls to resolve near-wall flow gradients. Mesh independence was verified using three grid resolutions: 3.5 million (coarse), 6.5 million (medium), and 8.5 million (fine) elements, following established grid refinement ratios [12].

Figure 4 shows the hexahedral mesh structure with prism layers near the wall boundaries. Figure 5 presents normalized velocity profiles along the vertical centerline for all three meshes. The medium and fine meshes produce nearly identical results, with maximum deviations of less than 2%, while the coarse mesh exhibits deviations exceeding 5% in the near-wall regions. These results confirm that the medium mesh (6.5 million elements) achieves grid-independent solutions. All subsequent simulations employ this medium mesh configuration.

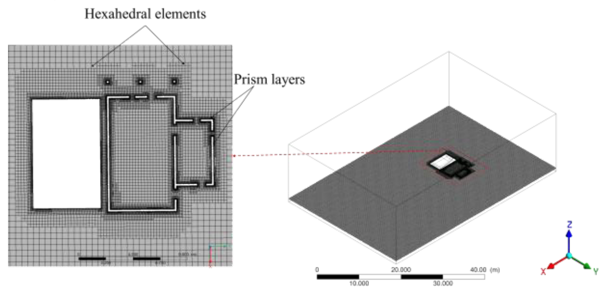

Fig.4. Mesh design of the indoor space of the computational domain by the hexahedral elements. 10-prism layers are adjacent to the building boundary wall.

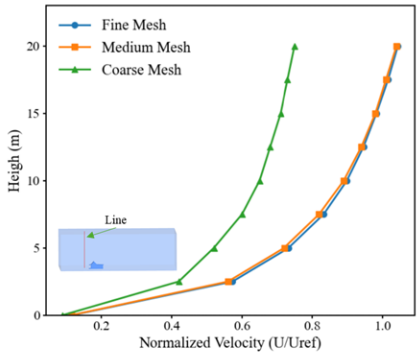

Fig.5. Grid independence testing for the front of the building based on the velocity profile at Line 1

3 Results

3.1. CFD simulation validation

Figure 6 illustrates the regression analysis comparing the simulated and measured outdoor air velocity and temperature. The scatter plots reveal a strong linear relationship between the CFD simulation results and the on-site measurements obtained from the METSENS550 Compact Weather Sensor, located near the case study building. This agreement indicates that the model effectively reproduces the diurnal variations of both parameters. The R^2 values of 0.89 for velocity and 0.90 for temperature demonstrate high predictive accuracy. The corresponding root mean squared errors (RMSE) of 0.10 m/s and 1.46°C indicate that the discrepancies between simulated and measured data are limited. Overall, the close agreement supports the suitability of the applied boundary conditions for subsequent indoor CFD simulations under the examined scenario.

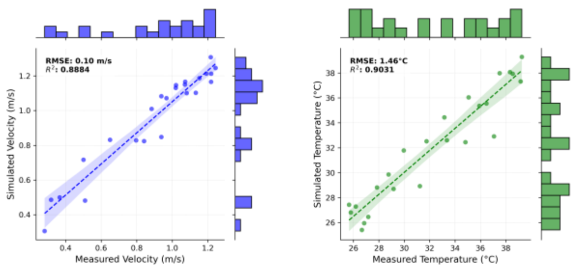

Fig.6. Regression plot comparing simulated (CFD simulation) and measured velocity and temperature

3.2. Velocity distribution

Figure 7 presents velocity distributions through vertical and horizontal cross-sections of the dwelling. The vertical cross-section (Figure 7a) reveals pronounced thermal stratification with maximum velocities approaching 3.0 m/s near upper window openings, decreasing substantially to near-stagnant conditions (0.0-0.5 m/s) at floor level. This vertical gradient indicates that buoyancy-driven circulation dominates the flow field, with warm air rising along heated surfaces while cooler incoming air descends after entry. The horizontal cross-section at occupant level (Figure 7b, z=1.5m) shows velocity magnitudes predominantly below 1.0 m/s throughout interior spaces, with localized peaks of 2.0-3.0 m/s confined to areas immediately adjacent to openings where cross-ventilation occurs between windward and leeward facades. Central occupied zones exhibit minimal air movement (0.0-0.5 m/s), with approximately 68% of the floor area experiencing velocities below 0.5 m/s, which is insufficient for thermal comfort enhancement through convective cooling according to ASHRAE Standard 55 guidelines (a minimum of 0.8 m/s is required). These low-velocity zones coincide spatially with elevated temperature regions (Figure 8), confirming that inadequate air circulation contributes to heat accumulation in interior spaces. The limited ventilation penetration explains why cool roof benefits manifest primarily through reduced conductive heat gain rather than enhanced ventilation cooling. The modest velocity magnitudes throughout the dwelling demonstrate that natural ventilation cannot provide sufficient air movement for effective heat removal when outdoor temperatures approach indoor conditions, underscoring the need for envelope-based interventions to address heat gain at its source.

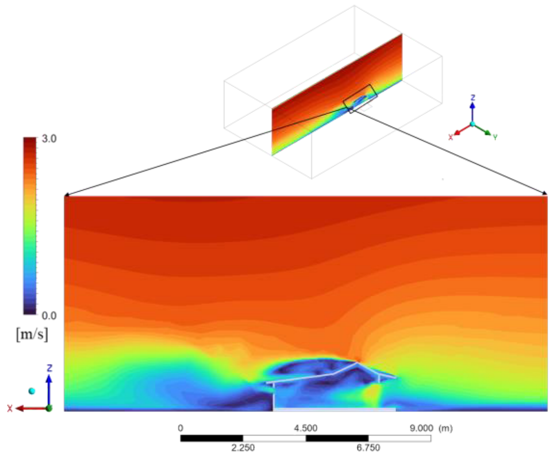

(a)

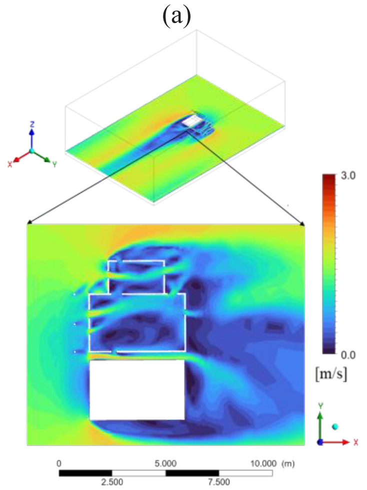

(b)

Fig.7. Velocity distribution inside building; (a) vertical cross-section; (b) horizontal cross-section (height = 1.5 m)

3.3. Temperature distribution

Figure 8 presents the 24-hour evolution of the area-averaged indoor air temperature for four roof albedo scenarios. Indoor temperatures reach their maximum values at 15:00, exhibiting a two- to three-hour lag after solar noon due to thermal mass effects. Peak temperatures are 35.0°C (α = 0.2), 34.8°C (α = 0.4), 34.6°C (α = 0.6), and 34.2°C (α = 0.8), yielding a 0.8°C reduction with cool roofs. The diurnal curve exhibits three phases. Morning heating (08:00-14:00) shows an 11°C temperature rise with minimal albedo differentiation below 0.5°C, indicating thermal mass dominance. The peak plateau (14:00–18:00) sustains maximum temperatures for four hours with maximum albedo effects reaching 0.8°C. Evening cooling (18:00-08:00) exhibits a gradual temperature decline, with scenario differences diminishing to below 0.2°C by midnight. All scenarios exceed the 32°C heat stress threshold for six to eight hours. Cool roofs reduce this duration by 1.5 hours (20% reduction) and decrease peak overheating from 3.0°C to 2.2°C above threshold (27% improvement). However, temperatures exceed 29°C for 11.5 to 13.0 hours across all scenarios, demonstrating that natural ventilation alone cannot maintain thermal comfort when outdoor temperatures approach those of the indoor environment.

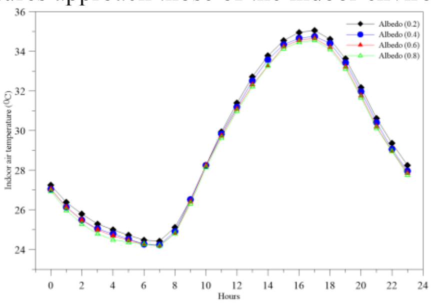

Fig.8. Diurnal evolution of indoor air temperature (area-averaged) for four roof albedo scenarios

Figure 9 presents horizontal temperature distributions at the occupant level (z = 1.5 m) at 13:00 for four albedo scenarios. Indoor temperatures range from 28°C near windows to 33-35°C in central zones. Peak temperatures decrease from 35°C (baseline, α=0.2) to 34.2°C (cool roof, α=0.8), yielding a 0.8°C reduction consistent with temporal analysis. Horizontal temperature gradients of 4-6°C persist across scenarios due to limited ventilation penetration. Central interior regions remain substantially warmer than perimeter zones near windows. The spatial temperature range decreases from 7°C to 6°C, representing a 14% reduction in thermal variation. Despite improvements, substantial interior areas exceed 30°C across all scenarios. Areas within 1m of windows experience temperatures 4-7°C lower than those outside, but represent only 20% of the floor area, demonstrating that natural ventilation combined with cool roofs cannot fully maintain thermal comfort during peak conditions.

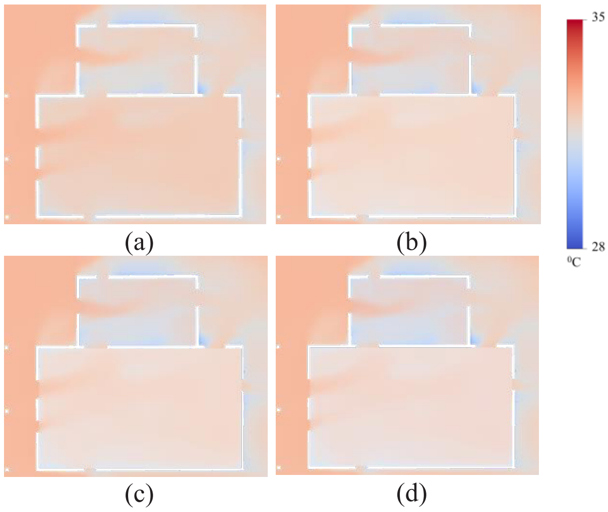

Fig. 9. Temperature distribution of horizontal cross-section (height = 1.5 m) at 13:00 (a) albedo=0.2; (b) albedo=0.4; (c) albedo=0.6; (d) albedo=0.8

3.4. Building heat balance components

To clarify how roof reflectivity affects indoor heat gain, the building's sensible heat balance was analyzed at 13:00, the period of maximum solar loading. Each component was derived from CFD-calculated fluxes: short-wave solar absorption, long-wave exchange, conduction through the envelope, ventilation and infiltration, and transient storage within indoor air and surfaces. At the daily peak, the α=0.20 case dominated the load path, with roof solar absorption exceeding 520W/m^2, accounting for nearly half of the total sensible heat gain. As the albedo increased, the absorbed solar energy declined almost linearly, lowering the roof-surface temperature and subsequent conduction into the zone. In the α = 0.80 case, roof absorption decreased by ~75%, resulting in a 7–8°C reduction in inner-surface temperature and a 60% decrease in conductive heat transfer. These changes account for the simulated 0.8°C decrease in peak indoor temperature and ≈ approximately 20% reduction in hours above 32°C. Ventilation and infiltration remained minor (< 5%), reflecting weak air movement (< 0.5 m s^{-1}). The transient storage term was positive during late morning and reversed during evening cool-down, consistent with the 2–3h lag between solar noon and indoor peak temperature.

Table 1. Sensible heat-flux components at 13:00h under different roof albedo scenarios (W)

Component (W)	α = 0.20	α = 0.40	α = 0.60	α = 0.80
Roof solar absorbed	2480	1920	1310	610
Walls solar absorbed	960	940	910	870
Windows solar absorbed	420	410	395	380
Ventilation sensible	185	180	178	176

Infiltration sensible	94	93	91	89
Storage (air + surfaces)	310	270	240	210
Conduction – roof	910	720	520	360
Conduction – walls	250	245	240	230

The results confirm that roof absorption and conduction account for more than 60% of the total sensible load. Increasing albedo interrupts this dominant solar-to-conduction pathway, producing measurable cooling even without enhanced ventilation. Comparable reductions in surface and indoor temperatures have been reported in field studies of reflective-roof retrofits underscoring that cool roofs provide an effective and low-cost means to mitigate indoor overheating in low-insulated dwellings [13–15].

4. Discussion

4.1. Implications for heat vulnerability and energy burden

Our integration of simulation, field measurements, and aerial thermography provides convergent evidence on how the optical properties of roofs shape indoor heat exposure in San Antonio's older housing stock. The validated CFD model accurately reproduced the observed dynamics (R^2 = 0.90 for air temperature and R^2 = 0.89 for air velocity), indicating that the model effectively captures the diurnal coupling between roof gains, indoor conduction, and weak cross-ventilation. Consistent with prior field evaluations, increasing roof reflectance lowers roof surface temperatures and the resulting conductive heat influx to the zone, thereby reducing peak indoor temperatures and time above high-risk thresholds. Field and monitoring studies report large roof surface cool-downs and measurable indoor/energy impacts, for example, a paired-home experiment in California documented cooler roof/attic profiles and reduced ceiling and duct heat gains after installing a cool tile roof, with instrumentation details and time-of-day effects reported explicitly [14]. Similarly, the drone thermal images collected in the context of the City of San Antonio's Cool Roof initiative [16] (Figure 10) illustrate the same mechanism in situ: the unshaded cool roof area (left) averaged 37.7°C, while the unshaded dark asphalt shingle roof (right) averaged 40.3°C, a 2.6°C difference under the same midday condition. These observations align with longstanding monitoring and program evaluations, which show that solar-reflective roofs stay markedly cooler in the sun and reduce conductive gains into buildings, mechanisms that translate into lower cooling loads and peak demand [17]. In various climates, reflective retrofits have yielded surface temperature reductions of tens of degrees and indoor temperature reductions of 0.5–2°C, depending on construction and ventilation conditions [14,18]. From an equity perspective, these results speak directly to the unequal distribution of heat risk in U.S. cities. Empirical studies have shown that lower-income and historically redlined neighborhoods experience systematically higher summer SUHI intensity and heat exposure, thereby concentrating risk among energy-burdened households [19,20]. For such homes, often single-story, under-insulated, and reliant on natural ventilation, sequenced passive retrofits provide the best ratio of benefit to cost: (1) apply high-albedo coatings to interrupt the dominant "solar-to-conduction" pathway; (2) add attic/roof insulation to suppress residual conductive gains; and (3) supplement with targeted, time-limited mechanical cooling during peak hours. This prioritization is consistent with field and modeling evidence that reflective envelopes reduce roof/attic temperatures and cooling energy while avoiding large new electrical loads at critical times [14,17]. In this housing typology, high-albedo roofs are necessary but not sufficient. Because roof solar absorption and roof conduction dominate peak sensible heat gains, combining a high-albedo roof with modest attic/roof insulation would further reduce conductive heat transfer, even during hot periods. Targeted exterior shading can also limit solar gains through glazing and reduce radiant load in occupied areas. When implemented together, cool roofs, insulation, and selective shading provide a practical retrofit package for older, under-insulated homes by addressing overheating driven by roofs and windows. When paired with modest insulation and basic shading, they can substantially reduce peak exposure and energy burden for heat-vulnerable households, an adaptation pathway supported by both our validated CFD and independent field literature.

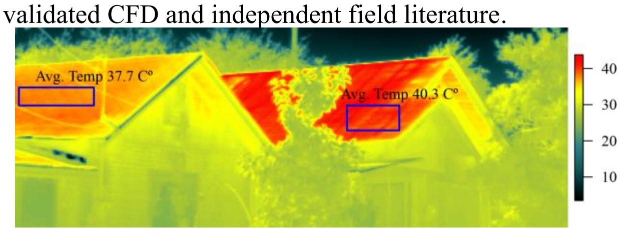

Fig. 10. UAV-based thermal imagery of roof surface temperature from the City of San Antonio Cool Roof Program (2025)

4.2. Policy relevance and equity consideration

The retrofit of cool-roof systems offers more than thermal regulation: by lowering interior heat loads and reducing cooling demand, such interventions also diminish associated power-plant emissions, thereby contributing to improved indoor air quality and potential health outcomes. Recent studies indicate that reflective surface interventions, such as cool roofs and cool pavements, effectively lower surface temperatures but yield modest reductions in near-surface air temperature. Consequently, municipal heat-mitigation policies should combine reflective coatings with vegetation, urban shading, and material-durability measures to enhance human thermal comfort and surface longevity [21,22]. Program targeting should prioritize census tracts with elevated heat exposure, high poverty rates, and aging or under-maintained housing while incorporating energy-burden indicators to strengthen equity outcomes [19,20,23].

Accurate spatial targeting is essential, as aggregation bias can misidentify heat hotspots and misallocate resources [24]. High-resolution thermal and land-use data should therefore guide site selection and investment prioritization [24]. Long-term monitoring of albedo degradation and maintenance cycles, coupled with quasi-experimental evaluations (e.g., difference-in-differences designs between treated and control sites), will improve the evidence base for program performance and cost effectiveness [21,22]. Aligning retrofit programs with the City's Strategic Housing Implementation Plan and Equity Atlas can integrate cooling strategies with housing-quality improvements and code-enforcement initiatives [23]. Maintaining and finding energy-efficient ways to do home retrofits is imperative not only for San Antonio, but for any other city facing an affordability crisis. As older stock is often the more affordable stock [25], programs and efforts to maintain it will help preserving affordable stock as a short-term solution (or non-aggravating strategy) in the meantime longer strategies of housing construction take place. Finally, having rigorous studies about the impact of these programs will help create public trust that bond and public dollars are spent efficiently to make a real difference in communities.

4.3. Limitations and future research directions

This study analyzed one representative single-family home under typical summer conditions in the San Antonio region to enhance the external validity of findings, future work should apply the validated CFD model across a broader array of housing types (e.g., multi-unit, mobile homes, varying insulation levels) and over multiple seasonal and weather-variability scenarios. Model validation focused on near-building outdoor temperature and wind speed to verify boundary-condition fidelity. To address the limitation, full indoor validation will be conducted using multi-point indoor monitoring during the diurnal cycle at multiple heights and locations to evaluate stratification and reduce uncertainty in room-scale predictions. Previous studies warn that retrofit outcomes often diverge from expected energy savings due to behavioral factors and envelope-householder interactions [26]. Therefore, future research should integrate humidity and pollutant-transport modules with the CFD framework to evaluate indoor air-quality outcomes (e.g., ventilation rates, pollutant dispersion) in addition to thermal comfort and energy performance. Such coupling would enable quantification of ventilation effectiveness and pollutant exposure, thereby strengthening the link between retrofit intervention and occupant health.

4 Conclusion

This study analysis showed that increasing roof albedo from 0.20 to 0.80 reduced roof solar absorption by 75 % and conductive heat transfer by 60 %, which lowered the indoor peak temperature by approximately 0.8°C. Consequently, the duration of indoor temperatures exceeding 32°C decreased by about 20 % (1.5 h). These results demonstrate that high-albedo cool-roof coatings provide a measurable, cost-effective means of improving thermal comfort in single-family homes located in ASHRAE Climate Zone 2A. Because roof solar gain accounts for more than half of the sensible heat load in under-insulated dwellings, policymakers can prioritize cool-roof installations as the first retrofit step in climate-zone 2A programs. When combined with modest attic insulation and targeted shading, the strategy can further reduce peak indoor temperatures and energy demand. Equity considerations are essential: low-income neighborhoods often contain older, poorly insulated homes that experience the greatest heat stress. Implementing subsidized cool-roof retrofits in these areas can alleviate disproportionate exposure to extreme temperatures and reduce energy-burden disparities. Overall, the study provides quantitative evidence to support the inclusion of high-albedo roof coatings in building-code updates and retrofit incentive schemes aimed at enhancing thermal resilience and promoting environmental justice.

Acknowledgement

The authors gratefully acknowledge the Historic Westside Residents Association (HWRA) and the Esperanza Community Land Trust for their collaboration and for providing access to the case study building. The authors are also grateful for the support of the Climate-Sensitive Design Lab (CSDL), a research arm of the School of Architecture and Planning at the University of Texas at San Antonio.

References:

[1] He Y, Yu H, Ozaki A, Dong N. Thermal and energy performance of green roof and cool roof: A comparison study in Shanghai area. J Clean Prod 2020;267:122205. https://doi.org/10.1016/J.JCLEPRO.2020.122205

[2] Costanzo V, Evola G, Marletta L. Energy savings in buildings or UHI mitigation? Comparison between green roofs and cool roofs. Energy Build 2016;114:247–55. https://doi.org/10.1016/J.ENBUILD.2015.04.053

[3] Coutts AM, Daly E, Beringer J, Tapper NJ. Assessing practical measures to reduce urban heat: Green and cool roofs. Build Environ 2013;70:266–76. https://doi.org/10.1016/J.BUILDENV.2013.08.021.

[4] Izquierdo S, Rodrigues M, Fueyo N. A method for estimating the geographical distribution of the available roof surface area for large-scale photovoltaic energy-potential evaluations. Solar Energy 2008;82:929–39. https://doi.org/10.1016/J.SOLENER.2008.03.007

[5] Bevilacqua P. The effectiveness of green roofs in reducing building energy consumptions across

different climates. A summary of literature results. Renewable and Sustainable Energy Reviews 2021;151:111523. https://doi.org/10.1016/J.RSER.2021.111523.
[6] Mohammed A, Khan A, Khan HS, Santamouris M. On the energy impact of cool roofs in Dubai. Solar Energy 2024;272:112447. https://doi.org/10.1016/J.SOLENER.2024.112447.
[7] Seifhashem M, Capra BR, Milller W, Bell J. The potential for cool roofs to improve the energy efficiency of single storey warehouse-type retail buildings in Australia: A simulation case study. Energy Build 2018;158:1393–403. https://doi.org/10.1016/J.ENBUILD.2017.11.034
[8] Elnabawi MH, Hamza N, Raveendran R. 'Super cool roofs': Mitigating the UHI effect and enhancing urban thermal comfort with high albedo-coated roofs. Results in Engineering 2023;19. https://doi.org/10.1016/j.rineng.2023.101269.
[9] Yang X, Gou Z, Chau HW. A decision framework for multi-dimensional analysis of roof retrofit scenarios to mitigate urban heat Island effects and enhance energy efficiency. Sustain Cities Soc 2025;130. https://doi.org/10.1016/j.scs.2025.106591.
[10] Hashemi F, Adib M. Examining thermal inequities: Land surface temperature, social vulnerability, and historical redlining in San Antonio, TX. Urban Clim 2024;55:101960. https://doi.org/10.1016/J.UCLIM.2024.101960.
[11] Tanaka H, Yoshie R, Hu C-H. Uncertainty in Measurements of Velocity and Concentration around a Building. Journal of Web Engineering 2006.
[12] Lee M, Park G, Park C, Kim C. Improvement of Grid Independence Test for Computational Fluid Dynamics Model of Building Based on Grid Resolution. Advances in Civil Engineering 2020;2020:8827936. https://doi.org/10.1155/2020/8827936.
[13] Akbari H, Pomerantz M, Taha H. Cool surfaces and shade trees to reduce energy use and improve air quality in urban areas. Solar Energy 2001;70:295–310. https://doi.org/10.1016/S0038-092X(00)00089-X.
[14] Rosado PJ, Faulkner D, Sullivan DP, Levinson R. Measured temperature reductions and energy savings from a cool tile roof on a central California home. Energy Build 2014;80:57–71. https://doi.org/10.1016/J.ENBUILD.2014.04.024
[15] Santamouris M, Yun GY. Recent development and research priorities on cool and super cool materials to mitigate urban heat island. Renew Energy 2020;161:792–807. https://doi.org/10.1016/J.RENENE.2020.07.109.
[16] Under 1 Roof - City of San Antonio n.d. https://www.sa.gov/Directory/Departments/NHSD/Housing-Support/Repair/Under-1-Roof (accessed November 8, 2025).
[17] Akbari H, Levinson R, Rainer L. Monitoring the energy-use effects of cool roofs on California commercial buildings. Energy Build 2005;37:1007–16. https://doi.org/10.1016/J.ENBUILD.2004.11.013
[18] Synnefa A, Santamouris M, Akbari H. Estimating the effect of using cool coatings on energy loads and thermal comfort in residential buildings in various climatic conditions. Energy Build 2007;39:1167–74. https://doi.org/10.1016/J.ENBUILD.2007.01.004
[19] Hsu A, Sheriff G, Chakraborty T, Manya D. Disproportionate exposure to urban heat island intensity across major US cities. Nature Communications 2021 12:1 2021;12:1–11. https://doi.org/10.1038/s41467-021-22799-5.
[20] Quang Van T, Najafian P, Hashemi F, Morakinyo TE, López Ochoa E. Year-round heat exposure and structural spatial vulnerability: A case study of San Antonio, Texas. Sustain Cities Soc 2025;135:107021. https://doi.org/10.1016/j.scs.2025.107021.
[21] Samer D, Neil D, Wei Z, Eseban LO, Ryun L. Case study: Evaluation of cool pavement surface treatments in the City of San Antonio, Texas. AM3P 2025, Vienna: TU Wien, E230-03 Road Engineering, Wien; 2025, p. 374–7. https://doi.org/10.34726/10561.
[22] Debbage N, Zhai W, Ochoa EL, Lee J, Pineda A, Jones E, et al. Evaluating the Urban Heat Mitigation Potential of the San Antonio Cool Pavement Pilot Program EXECUTIVE SUMMARY. City of San Antonio Office of Sustainability: 2024.
[23] López Ochoa EA, Zhai W. Housing Perceptions and Code Enforcement: An Assessment of Demolition Orders Using Street View Imagery and Machine Intelligence. J Plan Educ Res 2025;45:531–48. https://doi.org/10.1177/0739456X241233976.
[24] López Ochoa E, Brown K, Lee RJ, Zhai W. Quantifying the spatial aggregation bias of urban heat data. Urban Clim 2024;55. https://doi.org/10.1016/j.uclim.2024.101945.
[25] Mallach A, Swanstrom T, Harrison A. Catalyzing a movement to produce greater public, private, and civil resources to improve housing conditions through home repair programs 2024.
[26] de Feijter FJ, van Vliet BJM. Housing retrofit as an intervention in thermal comfort practices: Chinese and Dutch householder perspectives. Energy Effic 2021;14:1–18. https://doi.org/10.1007/S12053-020-09919-8.